© 2021. Published by The Company of Biologists Ltd | Journal of Cell Science (2021) 134, jcs251637. doi:10.1242/jcs.251637

RESEARCH ARTICLE

Aberrant cytoplasmic localization of ARID1B activates ERK signaling and promotes oncogenesis

Srinivas Animireddy[1,2], Padmavathi Kavadipula[1], Viswakalyan Kotapalli[1], Swarnalata Gowrishankar[3], Satish Rao[4] and Murali Dharan Bashyam[1,*]

ABSTRACT

The ARID1B (BAF250b) subunit of the human SWI/SNF chromatin remodeling complex is a canonical nuclear tumor suppressor. We employed *in silico* prediction, intracellular fluorescence and cellular fractionation-based subcellular localization analyses to identify the ARID1B nuclear localization signal (NLS). A cytoplasm-restricted ARID1B-NLS mutant was significantly compromised in its canonical transcription activation and tumor suppressive functions, as expected. Surprisingly however, cytoplasmic localization appeared to induce a gain of oncogenic function for ARID1B, as evidenced from several cell line- and mouse xenograft-based assays. Mechanistically, cytoplasm-localized ARID1B could bind c-RAF (RAF1) and PPP1CA causing stimulation of RAF–ERK signaling and β-catenin (CTNNB1) transcription activity. ARID1B harboring NLS mutations derived from tumor samples also exhibited aberrant cytoplasmic localization and acquired a neo-morphic oncogenic function via activation of RAF–ERK signaling. Furthermore, immunohistochemistry on a tissue microarray revealed significant correlation of ARID1B cytoplasmic localization with increased levels of active forms of ERK1 and ERK2 (also known as MAPK3 and MAPK1) and of β-catenin, as well as with advanced tumor stage and lymph node positivity in human primary pancreatic tumor tissues. ARID1B therefore promotes oncogenesis through cytoplasm-based gain-of-function mechanisms in addition to dysregulation in the nucleus.

This article has an associated First Person interview with the first author of the paper.

KEY WORDS: ARID1B, NLS, c-RAF, ERK signaling, Wnt–β-catenin signaling

INTRODUCTION

The switch/sucrose non-fermentable (SWI/SNF) complex, originally discovered in yeast, functions as the primary chromatin remodeler in humans during ontogeny and adult life (Ho and Crabtree, 2010). It is a large (∼2 MDa) evolutionarily conserved multi-functional complex that uses energy from ATP hydrolysis to make nucleosomal DNA accessible for various regulatory proteins facilitating nuclear processes such as transcription, DNA repair and maintenance of chromosomal stability (Reisman et al., 2009). The multi-subunit complex includes one of two ATPase subunits, BRG1 (SMARCA4) or BRM (SMARCA2); five core components, namely INI1 (SMARCB1), BRG1-associated factor (BAF) 155 (SMARCC1), BAF170 (SMARCC2), BAF60 (SMARCD) and BAF57 (SMARCE1); and four mutually exclusive DNA-binding subunits, namely AT-rich interaction domain 1A (ARID1A, also known as BAF250a), ARID1B (BAF250b) (Wang et al., 1996), ARID2 (BAF200) (Yan et al., 2005) and GLTSCR1 or GLTSCR1L (also known as BICRA and BICRAL, respectively; Michel et al., 2018); in addition to up to ten varying accessory subunits. Inactivating mutations in genes encoding one of several SWI/SNF subunits are identified in up to 20% of cancers (Kadoch and Crabtree, 2013), attesting to the importance of this complex in tumor suppression.

ARID1B is a ubiquitously expressed subunit of the SWI/SNF complex (Inoue et al., 2002). ARID1B levels increase during differentiation of embryonic stem cells (Kaeser et al., 2008), and its ectopic expression induces *TP53* and *CDKN1A*, causing cell cycle arrest in HeLa cells (Inoue et al., 2011) and suggesting a possible tumor-suppressor function. ARID1B loss-of-function events including mutations (Fujimoto et al., 2012), chromosomal rearrangements (Sausen et al., 2013) and DNA methylation (Khursheed et al., 2013) are reported in several cancer types. In a previous study, we described a tumor-suppressor role for nuclear ARID1B in pancreatic cancer (PaCa) (Khursheed et al., 2013). Here, we report the identification and characterization of the ARID1B nuclear localization signal (NLS). Surprisingly, an NLS-mutant version of ARID1B localized to the cytoplasm and stimulated RAF–ERK signaling and β-catenin (CTNNB1) transcription activity causing increased tumorigenic features in pancreatic cancer cell lines grown in culture or as mouse xenografts. More importantly, cytoplasmic localization of ARID1B in pancreatic tumor samples correlated significantly with increased levels of active forms of ERK1/2 (used here to refer to ERK1 and ERK2, also known as MAPK3 and MAPK1, respectively) and β-catenin, as well as with advanced tumor stage and lymph node positivity.

RESULTS

ARID1B possesses a classical bipartite NLS

In order to determine the molecular basis for ARID1B nuclear location, we proceeded to define its NLS. GFP-tagged full-length ARID1B exhibited a predominant nuclear localization when tested using fluorescence [in three cell lines of different origins, namely HEK293 (kidney), U2OS (bone) and MIA PaCa-2 (pancreas)] and subcellular fractionation followed by immunoblotting (in HEK293) (Fig. 1A). Based on a comparison of subcellular localization exhibited by several truncated versions of ARID1B, the probable NLS was estimated to be located between the ARID and the BAF250_C domains (Fig. 1A; gray box). A computational search using cNLS mapper (http://nls-mapper.iab.keio.ac.jp) revealed several putative NLS sequences, of which the one with the highest score (amino acids 1357–1377; Table S1) localized within the region (Fig. 1B) predicted

[1]Laboratory of Molecular Oncology, Centre for DNA Fingerprinting and Diagnostics, Hyderabad 500039, India. [2]Graduate Studies, Manipal Academy of Higher Education, Manipal 576104, India. [3]Apollo Hospitals, Hyderabad 500033, India. [4]Krishna Institute of Medical Sciences, Hyderabad 500003, India.

*Author for correspondence (bashyam@cdfd.org.in; bashyam69@gmail.com)

S.G., 0000-0002-4760-6259; M.D.B., 0000-0002-1967-5249

Handling Editor: Daniel Billadeau
Received 15 July 2020; Accepted 16 December 2020

Journal of Cell Science (2021) 134, jcs251637. doi:10.1242/jcs.251637

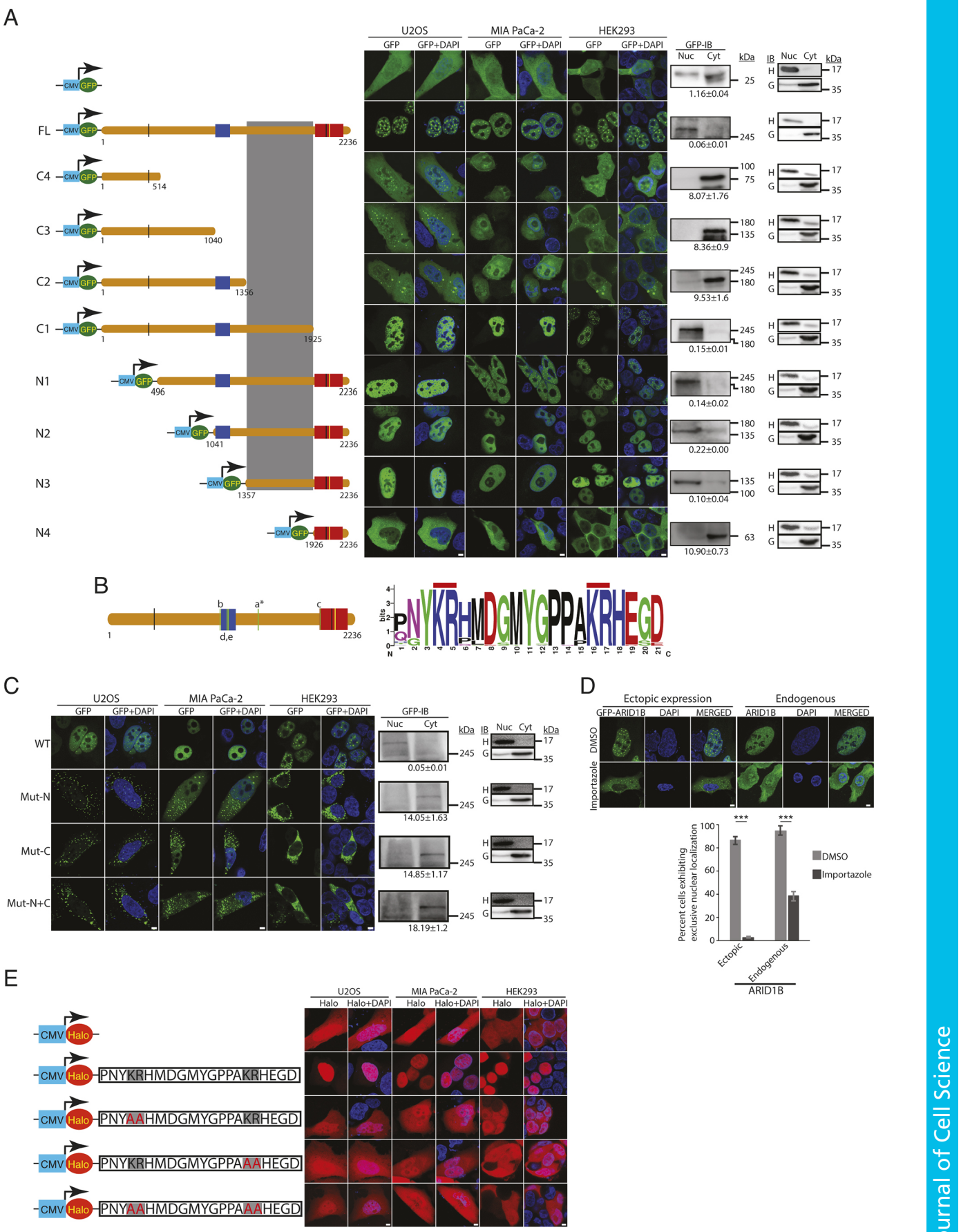

Fig. 1. See next page for legend.

Journal of Cell Science

Journal of Cell Science (2021) 134, jcs251637. doi:10.1242/jcs.251637

Fig. 1. Identification and characterization of the ARID1B NLS. (A) ARID1B truncations identify the putative region harboring the NLS. Diagrammatic depiction of constructs expressing GFP alone or GFP fused with full-length ARID1B or various ARID1B truncations generated in pDEST-N-EGFP is shown on the left. The ARID1B full-length construct is designated as FL and each C- and N-terminal deletion construct is labelled as C1–C4 and N1–N4, respectively. Blue, ARID domain; red, BAF250_C domain; black, LXXLL motif; yellow, B/C box motif; CMV, CMV promoter. A rectangular gray box depicts the probable location of the NLS. Intracellular localization of each GFP-tagged protein was detected in three different cell lines (as indicated) using GFP fluorescence (middle; GFP, green; DAPI, blue) and by immunoblotting performed separately for the nuclear and cytoplasmic fractions (only in HEK293; shown on the right). Mean±s.e.m. of cytoplasmic:nuclear ratios of the band intensities for each ARID1B derivative are shown below the respective GFP blot. (B) Left panel depicts location of five putative ARID1B NLS sequences (shown as thin green vertical bars and labelled a–e) identified using cNLS mapper. The askterisk indicates the position of the NLS sequence selected for characterization. The right panel depicts the consensus ARID1B NLS sequence derived using WebLogo with default settings, based on the alignment of ARID1B amino acid sequences from 42 vertebrate species (Fig. S1) using Clustal Omega. Each of the two highly conserved basic amino acid clusters (lysine-arginine) are indicated by red lines. (C) Validation of the ARID1B NLS. Representative results from transfected cells showing GFP fluorescence in the indicated cell lines (GFP, green; DAPI, blue) and GFP immunoblotting performed separately on nuclear and cytoplasmic fractions (only in HEK293). Mean±s.e.m. of cytoplasmic:nuclear ratios of the band intensities for each ARID1B derivative are shown below the respective GFP blot. WT, full-length ARID1B; Mut-N, full length ARID1B harboring mutated N-terminal basic amino acid cluster (AA instead of KR); Mut-C, full-length ARID1B harboring mutated C-terminal basic amino acid cluster (AA instead of KR); Mut-N+C, full-length ARID1B harboring mutated N- and C-terminal basic amino acid clusters. (D) Evaluation of ARID1B intracellular localization following importazole treatment on U20S cells using GFP fluorescence (green, left panels) and ARID1B antibody-based immunofluorescence (green, right panels) analyses. DAPI staining of nuclei is shown in blue. The graph depicts results from fluorescence quantitation. Data are presented as mean±s.d. (E) ARID1B NLS peptide alone can translocate a fused reporter (Halo tag) into the nucleus. Diagrammatic representation of each NLS peptide variant expression construct is shown on the left (the basic amino acid clusters are indicated by gray shading, and the mutant residues are indicated in red color). Fluorescence signal from representative cells expressing the particular variant is shown on the right (Halo, red; DAPI, blue). Nuc, nuclear fraction; Cyt, cytoplasmic fraction; IB, immunoblotting; H, Histone H3 immunoblotting as a positive control for the nuclear fraction; G, GAPDH immunoblotting as a positive control for the cytoplasmic fraction. Scale bars: 5 µm. Each result is based on at least three independent experiments. ***P<0.001 (unpaired Student's t-test).

by the truncation constructs. This putative 21-amino-acid sequence appeared to belong to the classical bipartite NLS family that is defined by two clusters of basic amino acids (lysine-arginine in this case) separated by a spacer region of 9–12 amino acids (10 in this case). Sequence alignment of human ARID1B (Uniprot ID: Q8NFD5) with its orthologs from 41 metazoan species (Fig. S1A) followed by WebLogo-based (weblogo.berkeley.edu) identification of the consensus (Fig. 1B) revealed significant conservation of the predicted NLS. The ARID1B NLS was also significantly similar (81% identity and 85.7% similarity; P=1.00749×10^{-9}) to that of its paralog ARID1A (Fig. S1B). We further validated the authenticity of this predicted NLS by confirming nuclear localization of another ARID1B truncation construct encompassing amino acids 1 to 1378 (Fig. S1C).

Alanine substitutions in either one or both basic amino acid clusters caused ARID1B to be significantly redistributed to the cytoplasm (Fig. 1C). Nuclear localization achieved through the classical (mono or bipartite) NLS is regulated by the importin α/β pathway (Lange et al., 2010). Importazole (an importin β blocker; Soderholm et al., 2011) treatment caused a significant reduction in nuclear localization of ectopically expressed as well as endogenous ARID1B (Fig. 1D; Fig. S1D), providing further evidence towards the authenticity of the predicted NLS. We ruled out the possibility of cytoplasmic localization of the ARID1B-NLS mutant (Mut-N+C from Fig. 1C) being a result of increased nuclear export by evaluating effect of leptomycin B treatment (Fig. S1E). Finally, NLS peptides harboring alanine substitutions in either or both of the two basic amino acid clusters lost the ability of nuclear translocation exhibited by the wild-type NLS peptide (Fig. 1E; Fig. S1F). These results provide support for authenticity of the predicted NLS sequence and suggest that the predicted NLS was not only necessary but perhaps sufficient to translocate an unrelated protein into the nucleus.

Similar to a null mutant, cytoplasm-localized ARID1B loses tumor-suppressor and transcription regulatory functions

ARID1B is a classical nuclear tumor suppressor that causes cell cycle arrest and/or senescence by inducing transcription of *CDKN1A* and *TP53* (Inoue et al., 2011; Tordella et al., 2016). Because transcription activation and tumor suppression mediated by ARID1B are nuclear activities, an ARID1B-NLS mutant localized to the cytoplasm was expected to be compromised in these canonical functions. In a previous study, we reported ability of ARID1B to induce senescence in MIA PaCa-2 cells (Khursheed et al., 2013). Ectopic expression of the cytoplasm-localized version of ARID1B severely compromised senescence induction when compared to the effect of expression of wild-type ARID1B in MIA PaCa-2 (Fig. 2A), as expected. We next evaluated status of canonical tumor-suppressive transcriptional targets of ARID1B. The ARID1B-NLS mutant was significantly restricted in its ability to transcriptionally activate *CDKN1A* (p21) and *TP53* in both MIA PaCa-2 and PANC-1 cells (Fig. 2B,C), corroborated further using a *CDKN1A* promoter–luciferase assay (Fig. 2D). We also tested induction of *CDKN1B* (p27), a well-established inducer of senescence not previously shown to be regulated by ARID1B or the SWI/SNF complex. Interestingly, wild-type ARID1B caused significant induction of *CDKN1B* (p27) at transcript and protein levels (Fig. 2B,C), confirmed further using promoter–luciferase assay (Fig. 2D). The cytoplasmic form of ARID1B was, however, unable to induce *CDKN1B* (p27) (Fig. 2B–D).

Unlike a null mutant, cytoplasm-localized ARID1B exhibits oncogenic functions

We confirmed the ability of wild-type ARID1B to cause reduction in cell growth and viability (Inoue et al., 2011; Tordella et al., 2016) in MIA PaCa-2 cells (Fig. 2E,F). Surprisingly however, the cytoplasmic form of ARID1B appeared to exhibit a neo-morphic function causing a significant increase in cell growth and viability in the same assays (Fig. 2E,F) as well as in cell migration assays (Fig. 2G).

Given that wild-type (nuclear) ARID1B inhibits β-catenin nuclear function (Vasileiou et al., 2015), we evaluated status of transcriptional activation mediated by β-catenin upon ectopic expression of the cytoplasmic version of ARID1B using two readouts of canonical Wnt–β-catenin signaling namely (1) *AXIN2* expression (Leung et al., 2002) and (2) TOP/FOPFlash promoter–luciferase assay (Ishitani et al., 1999). As expected, ectopic expression of wild-type ARID1B resulted in decreased β-catenin transcriptional activation function (Fig. 3A,B). Surprisingly, cytoplasm-restricted ARID1B caused a significant upregulation of β-catenin transcription activity (Fig. 3A,B). β-catenin nuclear entry is inhibited by a destruction complex that triggers proteasomal degradation of cytoplasmic β-catenin, which in turn is initiated by phosphorylation at Ser45 position of β-catenin caused by CK1 (Amit

Journal of Cell Science (2021) 134, jcs251637. doi:10.1242/jcs.251637

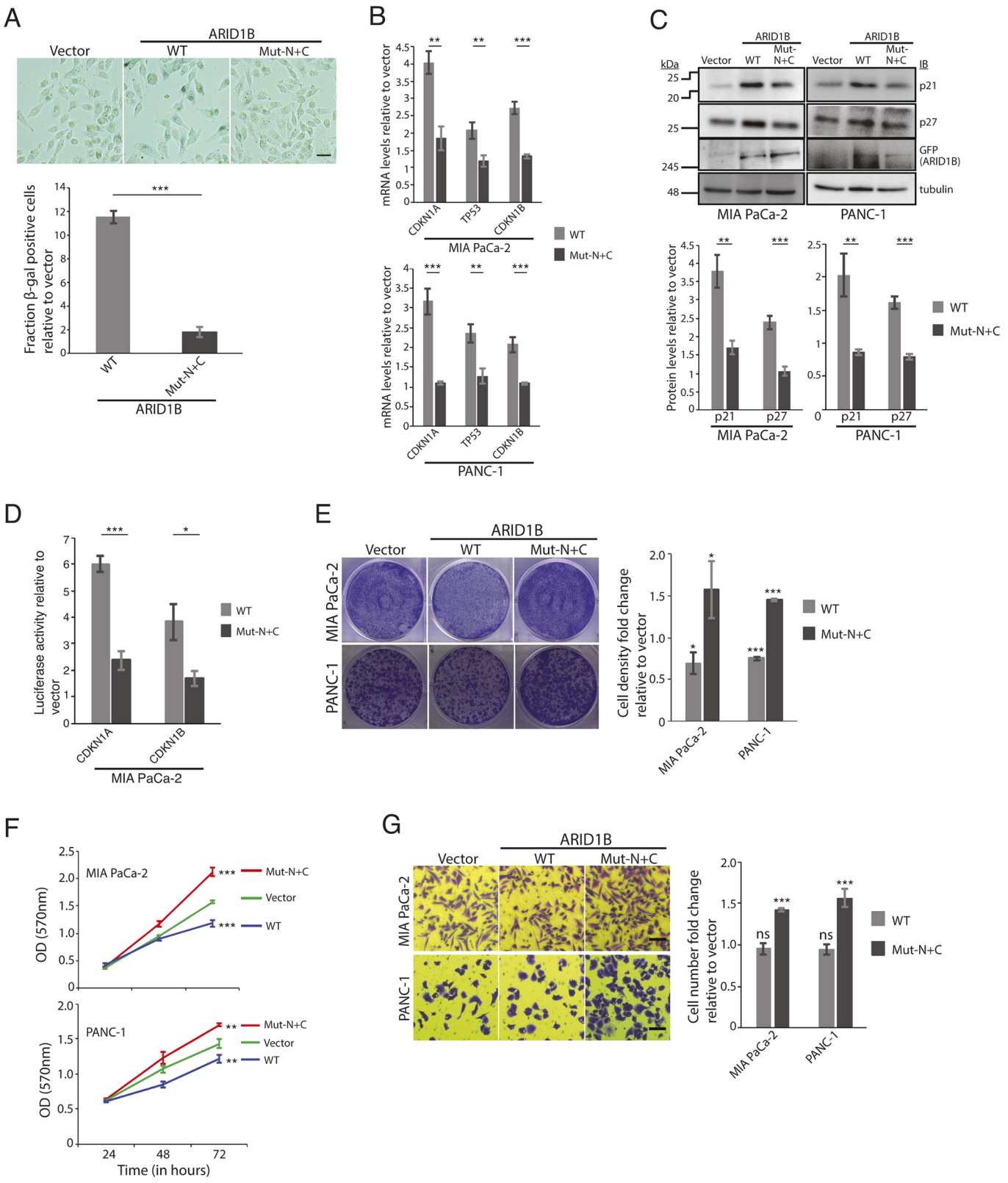

Fig. 2. See next page for legend.

et al., 2002). Cytoplasm-restricted (and not wild-type, nuclear) ARID1B caused an increase in the non-phosphorylated (active) form of β-catenin (Fig. 3C).

Thus, based on our work on PaCa cell lines, ARID1B appeared to exhibit a gain of oncogenic function when sequestered in the cytoplasm. We next tested tumor formation ability of PaCa cells

Journal of Cell Science

Journal of Cell Science (2021) 134, jcs251637. doi:10.1242/jcs.251637

Fig. 2. Cytoplasm-restricted ARID1B is compromised for transcription regulatory and tumor-suppressor functions but promotes oncogenic properties. (A) Senescence-associated β-galactosidase assay. Top panels show representative images of β-galactosidase staining of MIA PaCa-2 cells expressing the indicated ARID1B constructs, or a vector-only control (β-galactosidase-positive cells are indicated by black arrowheads), while the bottom panel shows quantitation. (B–D) ARID1B NLS mutant (Mut-N+C) is compromised to induce transcription of canonical tumor suppressor targets *CDKN1A* (p21) and *TP53*, as well as *CDKN1B* (p27), as measured by quantifying mRNA (B) and protein (C) levels, as well as through promoter–luciferase assays in the indicated cell lines (D). Tubulin is shown as a loading control in C. (E–G) Ectopic expression of the cytoplasmic version of ARID1B results in increased tumorigenic potential of pancreatic cancer cells as measured by Crystal Violet staining (E), MTT (F) and Transwell migration (G) assays. IB, immunoblotting; WT, nuclear (wild-type) ARID1B; Mut-N+C, cytoplasmic (NLS mutant) ARID1B (from Fig. 1C); Vector, empty-vector control. Quantitative data are presented as mean±s.d. Each result is based on at least three independent experiments. *P<0.05; **P<0.01; ***P<0.001; ns, not significant (unpaired Student's t-test). Scale bars: 20 µm in A, 30 µm in G.

harboring cytoplasmic ARID1B. Indeed, MIA PaCa-2 cells expressing the cytoplasmic form of ARID1B exhibited significantly increased tumor formation ability in xenograft assays performed in nude mice (Fig. 3D–F; Fig. S2A). Taken together, these observations suggest the first probable evidence for a gain of oncogenic function exhibited by cytoplasm-localized ARID1B.

Cytoplasm-localized ARID1B activates RAF–ERK signaling

The observed oncogenic gain of function exhibited by cytoplasm-localized ARID1B could be a result of cytoplasmic sequestration of other SWI/SNF components causing inactivation of this tumor-suppressive nuclear complex. In order to rule out this possibility, we evaluated the endogenous localization status of two core (BAF155 and BAF57), one ATPase (BRG1) and one accessory (BAF53A, also known as ACTL6A) constituents of SWI/SNF under the influence of ectopically expressed cytoplasmic form of ARID1B. As shown in Fig. 4, there did not appear to be any evidence for nuclear depletion or cytoplasmic accumulation of any of the four SWI/SNF components tested.

We next endeavored to obtain mechanistic insight into the possible neo-morphic function exhibited by cytoplasmic ARID1B. We utilized data available from a Halo tag-based pulldown–mass spectrometry screen performed with cytoplasmic form of ARID1B

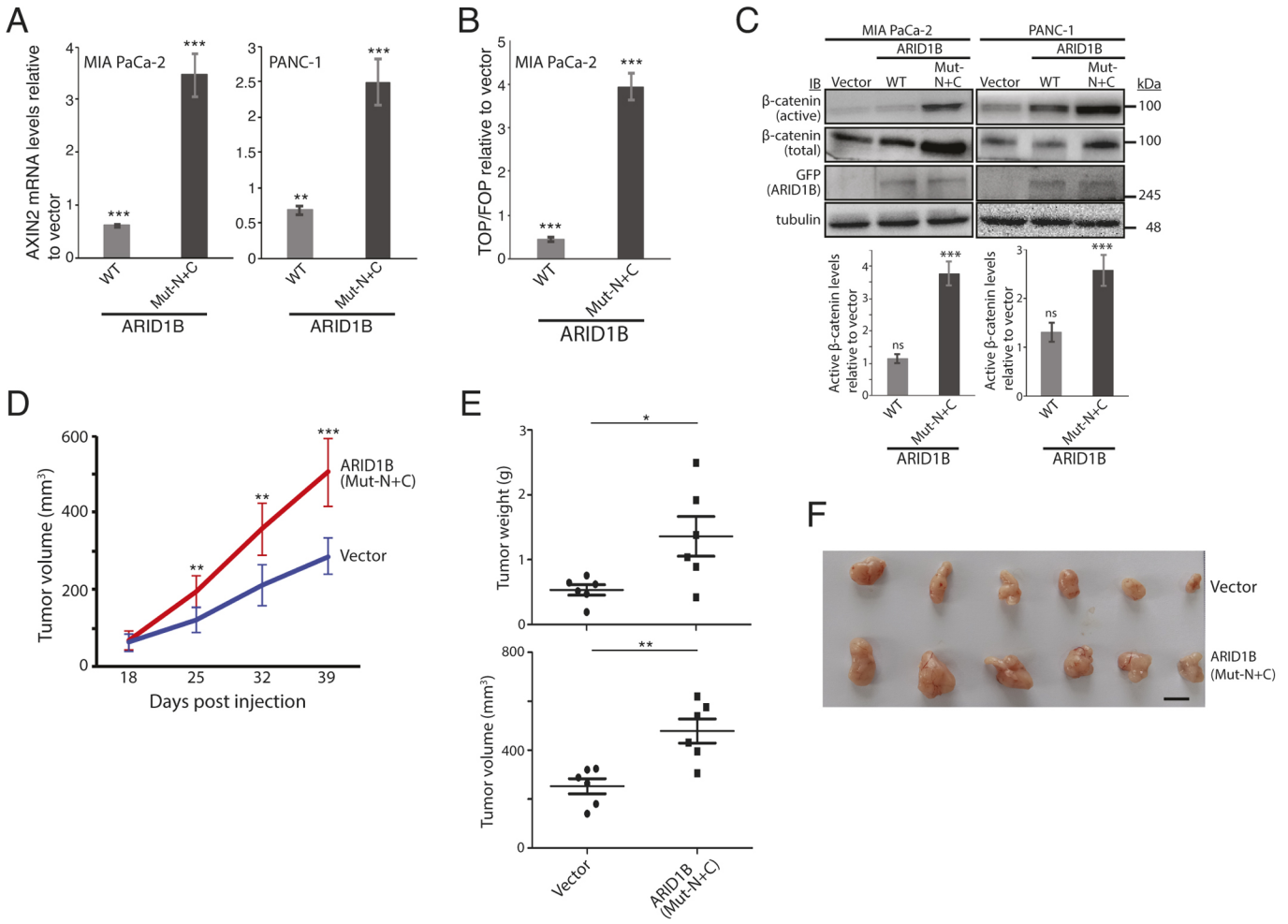

Fig. 3. Cytoplasm-restricted ARID1B promotes β-catenin transcription activation and oncogenesis in nude mice xenograft assays. (A–C) Cytoplasm-localized ARID1B elevates β-catenin transcription activity in the indicated cell lines, as evaluated by measuring *AXIN2* transcript levels (A) and relative promoter activity of TOPFlash over FOPFlash (B), as well as by quantitation of active (non-phosphorylated at Ser45) β-catenin levels (C). Tubulin is shown as a loading control in C. IB, immunoblotting. (D–F) Oncogenic role of cytoplasm-localized ARID1B in mouse xenograft tumors generated by MIA PaCa-2 cells expressing the cytoplasmic version of ARID1B or vector alone. Plot for change in tumor volume over time (mean for 6 animals) is shown in D. Plots for final tumor weight (top) and volume (bottom) (after excision) are shown in E. A picture of all 12 excised tumors is shown in F. WT, nuclear (wild-type) ARID1B; Mut-N+C, cytoplasmic (NLS mutant) ARID1B; Vector, empty-vector control. Quantitative data are presented as mean±s.d. Each result is based on at least three independent experiments. *P<0.05; **P<0.01; ***P<0.001; ns, not significant (unpaired Student's t-test). Scale bar: 10 mm.

Journal of Cell Science

Journal of Cell Science (2021) 134, jcs251637. doi:10.1242/jcs.251637

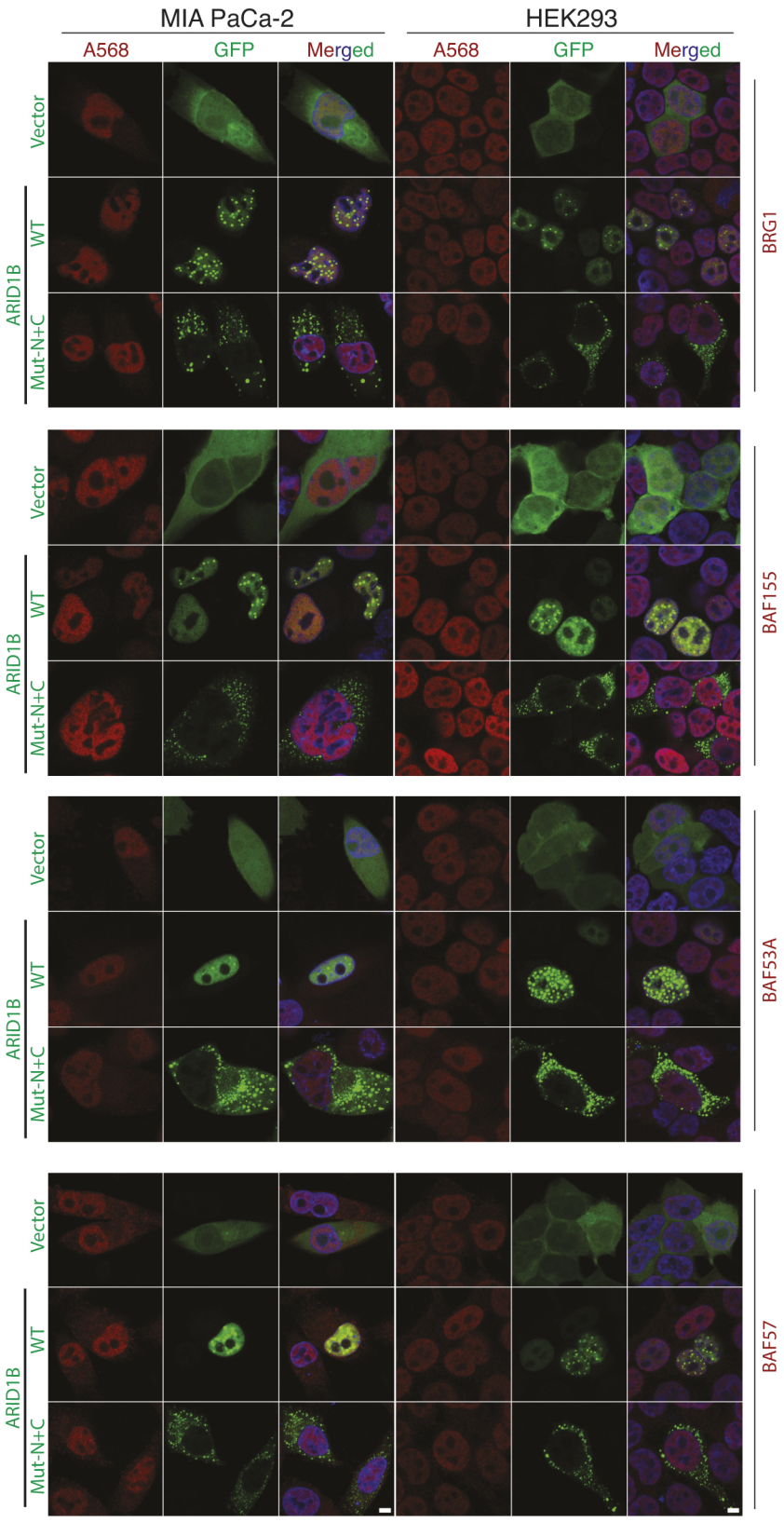

Fig. 4. Oncogenic gain of function exhibited by cytoplasm-localized ARID1B is not due to cytoplasmic sequestration of other SWI/SNF components. Intracellular localization of (endogenous) SWI/SNF components BRG1, BAF155, BAF53A and BAF57 was assessed through fluorescence-based analysis in the indicated cell lines. GFP-tagged ARID1B constructs and the empty-vector control are shown in green. Alexa Fluor 568 staining (A568) of the indicated SWI/SNF components is shown in red. The merged image includes DAPI stain (for nuclei, blue).; WT, nuclear (wild-type) ARID1B; Mut N+C, cytoplasmic (NLS mutant) ARID1B; Vector, empty-vector control. Scale bars: 5µm.

(Neetu Sharma, S.A., M.D.B., unpublished observations, used with permission) and, surprisingly, identified components and regulators of the RAF–ERK signaling pathway (following subtraction of interactors identified with the Halo tag alone), including a-RAF (ARAF) and c-RAF (RAF1), as potential interactors of cytoplasm-restricted ARID1B (Table S2). RAF–ERK signaling is a major driver of cell viability and growth and is also known to induce a migratory phenotype in epithelial cells (Plotnik et al., 2014). Of note, previous studies have implicated the RAF–ERK signaling cascade in direct phosphorylation of LRP6 leading to activation

Journal of Cell Science (2021) 134, jcs251637. doi:10.1242/jcs.251637

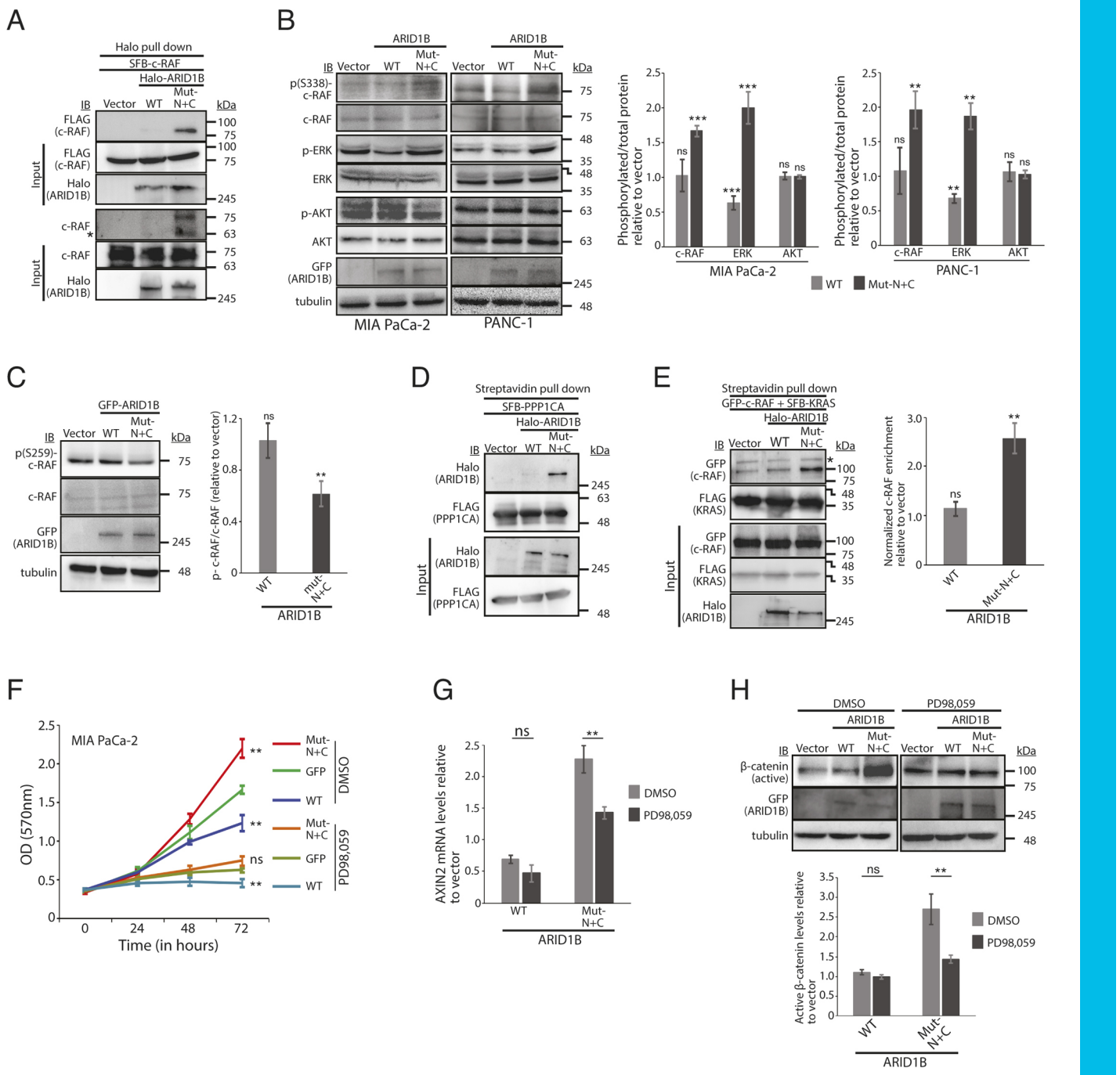

Fig. 5. Cytoplasmic ARID1B exhibits oncogenic gain of function by activating RAF–ERK signaling. (A) Interaction of Halo-tagged cytoplasmic ARID1B with ectopically expressed c-RAF (SFB–cRAF, detected using anti-FLAG tag antibody). (B) Cytoplasm-localized (and not nuclear) ARID1B activates c-RAF (phosphorylation at Ser 338) and ERK1/2 but not AKT in the indicated cell lines. Figure shows representative immunoblots and results of densitometric quantitation of active (phosphorylated, p):total ratios of respective proteins represented as fold induction over the levels obtained in the vector-only control. Extract from same transfection was used for the experiments depicted in Figs 3C and 5B (therefore the ARID1B and tubulin blots are the same). (C) Cytoplasm-localized ARID1B causes a decrease in inhibitory phosphorylation (at Ser259) of c-RAF. (D) Interaction of Halo-tagged cytoplasm-localized ARID1B with PPP1CA (SFB–PPP1CA). (E) Cytoplasm-restricted Halo-tagged ARID1B increases interaction between constitutively active (mutant) KRAS (SFB–KRAS) and GFP–c-RAF. (F–H) Oncogenic function exhibited by cytoplasm-localized ARID1B is dependent on ERK signaling. Results for MTT assays (F; performed as described in Fig. 2F), quantitation of *AXIN2* relative mRNA levels (G; performed as described in Fig. 3A) and quantitation of active (non-phosphorylated at Ser45) β-catenin levels (H; performed as described in Fig. 3C) upon treatment with the MEK1 and MEK2 inhibitor PD98,059 (20 µM) are shown. The asterisk in panels A and E indicates a non-specific band. Input blots in A,D,E represent 10% of the lysate. Tubulin is shown as a loading control in B,C,H. WT, nuclear (wild-type) ARID1B; Mut N+C, cytoplasmic (NLS mutant) ARID1B; Vector, empty-vector control; IB, immunoblotting. Quantitative data are presented as mean ±s.d. Each result is based on at least three independent experiments. ***P*<0.01; ****P*<0.001; ns, not significant (unpaired Student's *t*-test).

of canonical Wnt–β-catenin signaling (Cervenka et al., 2011) via inhibition of CK1 mediated β-catenin phosphorylation (Amit et al., 2002).

We confirmed ARID1B and c-RAF interaction by pulldown followed by immunoblotting (Fig. 5A; Fig. S2B) and fluorescence based colocalization studies (Fig. S2C). More importantly, ectopic

Journal of Cell Science (2021) 134, jcs251637. doi:10.1242/jcs.251637

expression of the cytoplasmic version of ARID1B resulted in a significant increase in the levels of the active form of c-RAF (phosphorylated at Ser338) and of ERK1/2 (Fig. 5B), although there was no effect on phosphorylated (active) AKT levels (Fig. 5B), confirming the specificity of RAF activation by the cytoplasmic ARID1B. Interestingly, wild-type ARID1B caused a significant reduction in phosphorylated ERK1/2 levels (Fig. 5B); Wnt–β-catenin signaling is known to activate ERK signaling (Zhang et al., 2014), and the observed reduction in active ERK is probably a result of downregulation of β-catenin transcription activation function by wild-type ARID1B. Removal of inhibitory phosphorylation at Ser259 is an initial step in the cascade of events leading to c-RAF activation. Ectopic expression of the cytoplasmic (but not nuclear) version of ARID1B resulted in decreased levels of the Ser259 phosphorylation in c-RAF (Fig. 5C). PPP1CA, the catalytic subunit of a protein phosphatase known to dephosphorylate c-RAF at Ser259 (Jaumot and Hancock, 2001), was also identified as a potential interactor of cytoplasmic ARID1B (Table S2). We confirmed the interaction of cytoplasmic ARID1B with PPP1CA (Fig. 5D). In the c-RAF activation cascade, removal of Ser259 phosphorylation is a prerequisite for binding of active RAS to c-RAF that in turn triggers the Ser338 phosphorylation of the latter (Kubicek et al., 2002). We confirmed a significant increase in the interaction between mutant (G12V; constitutively activated) KRAS and c-RAF in presence of the cytoplasmic (but not nuclear) form of ARID1B (Fig. 5E). These results appear to suggest that cytoplasmic ARID1B may potentiate alteration of regulatory phosphorylation dynamics of c-RAF, presumably via PPP1CA, providing a possible mechanistic insight into the mode of oncogenic action mediated by cytoplasmic ARID1B.

Finally, we tested the oncogenic gain of function exhibited by cytoplasmic ARID1B in the presence of PD98,059, an inhibitor of MEK1 and MEK2 (also known as MAP2K1 and MAP2K2, respectively) protein kinase activity responsible for phosphorylation of ERK1/2 downstream of activated RAF. Interestingly, presence of the inhibitor reduced the growth-potentiation effect of cytoplasmic ARID1B without affecting the growth-inhibitory effect of wild-type (nuclear) ARID1B (Fig. 5F), confirming independence of wild-type ARID1B function as well as specificity of PD98,059 action in the assay. Dependence of oncogenic function of cytoplasmic ARID1B on ERK signaling was further validated using SCH772984, a specific ERK inhibitor (Morris et al., 2013) (Fig. S2D), as well as by shRNA targeting ERK1/2 (Hong et al., 2009) (Fig. S2E). As already mentioned, previous studies have implicated the RAF–ERK signaling cascade in direct phosphorylation of LRP6, leading to activation of canonical Wnt–β-catenin signaling (Cervenka et al., 2011) via inhibition of CK1-mediated β-catenin phosphorylation (Amit et al., 2002). We therefore tested whether the activation of β-catenin transcription function in the presence of cytoplasmic ARID1B was dependent on activation of ERK signaling. Indeed, the increased levels of *AXIN2* transcript (Fig. 5G) as well as of active (non-phosphorylated) β-catenin (Fig. 5H) observed upon ectopic expression of the cytoplasmic form of ARID1B were significantly reduced in presence of PD98,059. Therefore, the primary effect of cytoplasm-localized ARID1B appears to be the activation of the RAF–ERK signaling cascade, which results in promoting a tumorigenic phenotype besides causing stabilization and activation of β-catenin transcription regulatory function.

Clinical relevance of the oncogenic role of cytoplasmic ARID1B

In order to garner clinical support for oncogenic gain of function mediated by cytoplasmic ARID1B, we carefully scrutinized the cBioPortal cancer somatic mutation database (cbioportal.org) for the presence of ARID1B mutations potentially affecting the NLS. The analysis revealed several ARID1B mutations, including splice-site, frame-shift and truncation mutations that could potentially inactivate the NLS. More importantly, we identified eight missense mutations located within the NLS (Fig. 6A; Table S3). Of these, one (p.D1377N) was also detected in a PaCa sample (Panc43; Table S4) that exhibited significant ARID1B cytoplasmic localization (Fig. 6A). The identification of ARID1B mutations within the NLS in tumor samples provided an opportunity to test whether these mutations could also re-distribute ARID1B into the cytoplasm and further cause a gain of oncogenic function. We first confirmed ability of mutant NLS peptides, each harboring either one of two missense mutations located within the NLS (p.R1361C and p.D1377N; Table S3), to stimulate cytoplasmic retention of a fused Halo tag in U2OS, MIA PaCa-2 and HEK293 cells (Fig. S2F). In addition, ectopically expressed ARID1B harboring the p.R1361C mutation was significantly redistributed into the cytoplasm (Fig. 6B; Fig. S2G). More importantly, mutant (R1361C) ARID1B promoted cell growth and viability, and migration potential (Fig. 6C–E) besides gaining the ability to bind c-RAF (Fig. 6F) causing stimulation of ERK activation (Fig. 6G). Finally, immunohistochemistry (IHC)-based evaluation performed on a PaCa tissue microarray (TMA) revealed significant correlation between ARID1B cytoplasmic localization and active forms of ERK1/2 and of (de-phosphorylated) β-catenin levels (Fig. 7A,B; Table S4). More importantly, ARID1B cytoplasmic localization correlated significantly with aggressive clinical features including advanced tumor stage and lymph-node positivity (Fig. 7C). Taken together, results obtained from tumor samples provide support for a clinical significance of cytoplasmic localization of ARID1B.

Given that ARID1B is a ubiquitously expressed protein implicated in several cancer types, the cytoplasmic localization of ARID1B was unlikely to be restricted to PaCa alone. However, no cytoplasmic staining was detected based on IHC performed on TMAs generated for adenocarcinomas of the esophagus (30 tumor and 10 normal samples), colon and rectum (120 tumor and 20 normal samples), as well as squamous carcinomas of the oral tongue (60 tumor and 25 normal samples) and esophagus (80 tumor and 15 normal samples) (data not shown). In contrast, we identified significant ARID1B cytoplasmic localization in breast cancer samples (Fig. S3, Table S5), suggesting a possible wider clinical significance of our novel discovery.

DISCUSSION

In this study, we report a novel oncogenic function for ARID1B; it appears to contribute to oncogenesis through a non-canonical cytoplasmic gain-of-function mechanism in addition to the well characterized mechanisms involving dysregulation in the nucleus (Fig. 8), thus adding to the growing list of cancer genes exhibiting a dual 'yin–yang' nature (Bashyam et al., 2019). Our discovery of c-RAF activation mediated by cytoplasmic ARID1B attests to the 'addiction' of pancreatic cancer cells for the RAF–ERK cell signaling cascade, as suggested previously (Waddell et al., 2015; Ying et al., 2012). Of interest, a synthetic lethality screen in a KRAS-mutant cell line revealed ARID1B as a significantly enriched gene (Luo et al., 2009). However, the precise molecular mechanism of c-RAF activation by cytoplasmic ARID1B remains to be dissected. Of note, additional proteins belonging to the RAF–ERK signaling pathway (IQGAP1 and -3) were identified in the ARID1B-interactor screen (Table S2).

Although extensively classified as a tumor suppressor, possible oncogenic roles for the SWI/SNF complex (Boulay

Journal of Cell Science (2021) 134, jcs251637. doi:10.1242/jcs.251637

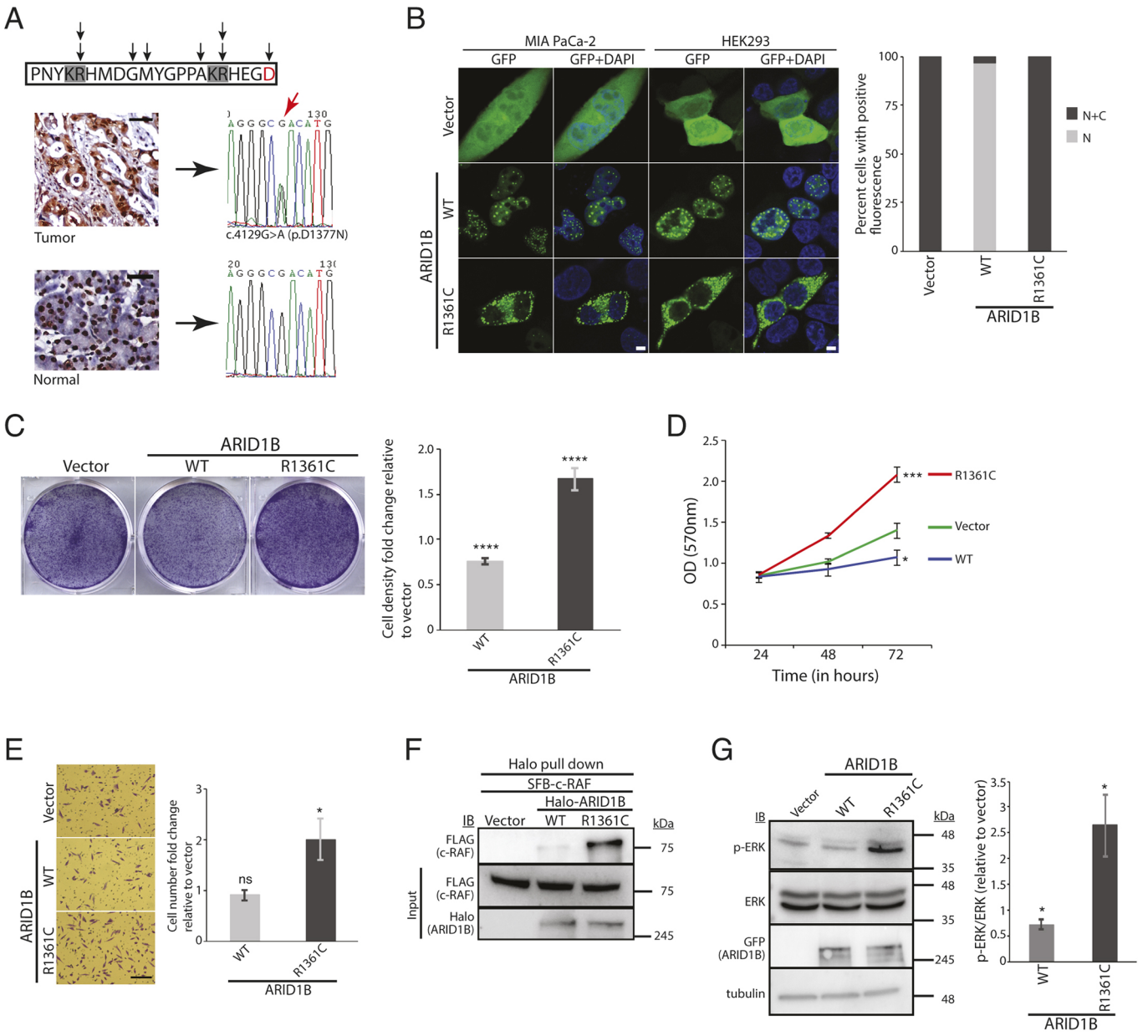

Fig. 6. Validation of gain of oncogenic function exhibited by ARID1B-NLS mutations identified from tumor samples. (A) Location of eight missense mutations within the ARID1B-NLS identified from the cBioPortal somatic cancer mutation database (top). Black arrows indicate the amino acids targeted by each mutation; double arrows indicate two distinct mutations affecting the same amino acid. The C-terminal most aspartic acid residue mutated in pancreatic tumor sample #Panc43 is depicted in red. List of mutations is given in Table S3. ARID1B IHC and DNA sequencing results for tumor and matched normal counterparts of #Panc43 exhibiting cytoplasmic localization of ARID1B (bottom). The mutant nucleotide in the electropherogram is indicated by a red arrow. (B–G) ARID1B harboring the R1361C mutation localizes to the cytoplasm (B), promotes tumorigenic features (C, plating efficiency as shown by Crystal Violet staining; D, MTT assay; E, Transwell migration assay), binds to c-RAF (F) and causes an increase in active ERK (phosphorylated, p-ERK) levels (G). WT, nuclear (wild-type) ARID1B; R1361C, full-length ARID1B harboring the p.R1361C mutation; Vector, empty-vector control; IB, immunoblotting. In B, GFP-tagged ARID1B constructs are shown in green and DAPI staining is shown in blue; N, positive for ARID1B nuclear staining; N+C, positive for ARID1B nuclear-plus-cytoplasmic staining. In F, input=10%. In G, tubulin is shown as a loading control. Quantitative data are presented as mean±s.d. Each result is based on at least three independent experiments. *P<0.05; ***P<0.001; ****P<0.0001; ns, not significant (unpaired Student's t-test). Scale bars: 30 µm in A, 5 µm in B and 100 µm in E.

et al., 2017; McBride et al., 2018; Pfister et al., 2015), as well as for its individual components (Shi et al., 2013), have been suggested. Gene fusion events involving the SS18 subunit of the BAF complex exhibiting oncogenic gain of function were reported in synovial sarcomas (Kadoch and Crabtree, 2013). Our study, however, is probably the first report of cytoplasmic localization-induced oncogenic gain of function exhibited by a component of the human SWI/SNF complex. Aberrant cytoplasmic localization of classical tumor suppressors, such as p16 (encoded by *CDKN2A*), has been reported previously (Romagosa et al., 2011). p110Rb (RB1) was shown to exhibit cytoplasmic localization in tumor samples leading to a possible gain of oncogenic function (Jiao et al., 2008). Similar non-canonical oncogenic functions have been shown for cytoplasm-localized p21 and p27 tumor-suppressor proteins (Blagosklonny, 2002; Koster et al., 2010).

Journal of Cell Science (2021) 134, jcs251637. doi:10.1242/jcs.251637

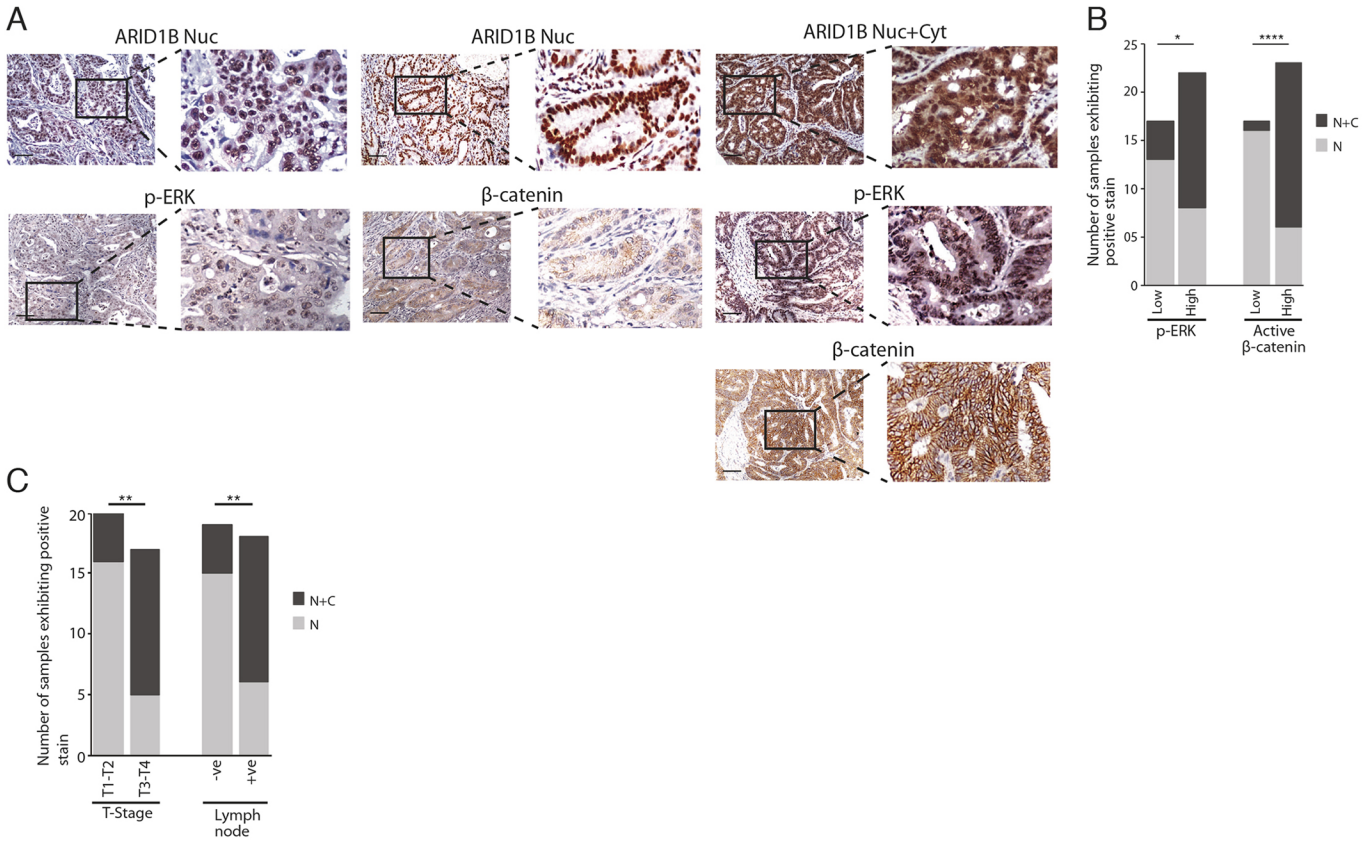

Fig. 7. ARID1B cytoplasmic localization correlates significantly with active forms of (phosphorylated) ERK1/2 and (non-phosphorylated) β-catenin as well as with advanced tumor stage and lymph node positivity in human primary pancreatic tumor samples. (A) Representative IHC images from the same sample exhibiting ARID1B (nuclear, Nuc) and phosphorylated ERK1/2 (p-ERK; low) staining (left); ARID1B (nuclear) and β-catenin (low) staining (middle); and ARID1B (nuclear plus cytoplasmic, Nuc+Cyt), p-ERK (high) and β-catenin (high) (right) staining. Boxes indicate regions shown in magnified images (right-hand image of each pair). Scale bars: 100 µm. (B) Graphical representation of the IHC results. (C) Graphical representation of the association of nuclear versus nuclear plus cytoplasmic stain with tumor stage or lymph node status (total of 37 samples). N, positive for ARID1B nuclear staining; N+C, positive for ARID1B nuclear plus cytoplasmic staining; T1-T2, low tumor stage; T3-T4, advanced tumor stage; –ve, negative; +ve, positive. *P<0.05; **P<0.01; ****P<0.00001 (two-tailed Fisher's exact test).

Of the two PaCa cell lines evaluated in this study, one (PANC-1) harbors the endogenous (nuclear) ARID1B, and thus it is possible that the observed gain of oncogenic functions exhibited by cytoplasmic ARID1B are due to an interference of the endogenous wild-type protein function by the ectopically expressed NLS mutant (similar to a dominant-negative effect). However, results obtained with the ARID1B null MIA PaCa-2 cells can only be explained by a gain of function of the cytoplasmic form unrelated to its nuclear function. Thus, ARID1B cytoplasmic localization appears to have an additional role to support tumorigenesis not due simply to a loss of its nuclear function. It will be interesting to test modes of regulation leading to ARID1B cytoplasmic localization, such as (1) via a nuclear export signal, (2) alterations in a binding partner, (3) posttranslational modifications, and others.

We detected ARID1B cytoplasmic localization in a significant proportion of breast cancer samples but not in cancers of the colon, rectum, esophagus or the oral tongue, suggesting that the results in pancreatic tumors were specific and neither artifactual nor a result of general perturbations in nuclear import/export machinery often observed in tumors. Interestingly, both breast and pancreatic cancers, unlike the other cancer types evaluated in this study, are classified as ductal adenocarcinomas.

The results presented here have potentially revealed a new facet of ARID1B and SWI/SNF biology. Is cytoplasmic localization causal to a hitherto undiscovered canonical function of ARID1B? Is this phenomenon exhibited by other SWI/SNF components? Most tumor types exhibit mono-allelic genetic lesions of SWI/SNF components, in contrast to bi-allelic inactivation observed for classical tumor suppressors; the tumor suppression is therefore presumed to be due to a dosage effect, and the 'residual' SWI/SNF nuclear function has been suggested to be an attractive therapeutic target (Mathur and Roberts, 2017). One can perhaps envisage a 'dosage' effect due to partial ARID1B cytoplasmic localization emanating for heterozygous mutations affecting the NLS. Given that SWI/SNF-deficient tumors are susceptible to bromodomain inhibitors acting through suppression of RAS–ERK signaling (Shorstova et al., 2019), and the recent demonstration of effective pancreatic tumor regression in genetically engineered mice as well as in patient-derived mouse xenografts when subjected to combined EGFR and c-RAF ablation (Blasco et al., 2019), the novel ERK-activating function of cytoplasm-localized ARID1B can be explored for therapeutic options.

MATERIALS AND METHODS

Cell line maintenance and their manipulations

MIA PaCa-2 and PANC-1 cells were procured from ATCC, whereas U2OS and HEK293 cells were kind gifts from Drs Rashna Bhandari and Sangita Mukhopadhyay (CDFD, Hyderabad, India), respectively. Cells, continuously

Journal of Cell Science (2021) 134, jcs251637. doi:10.1242/jcs.251637

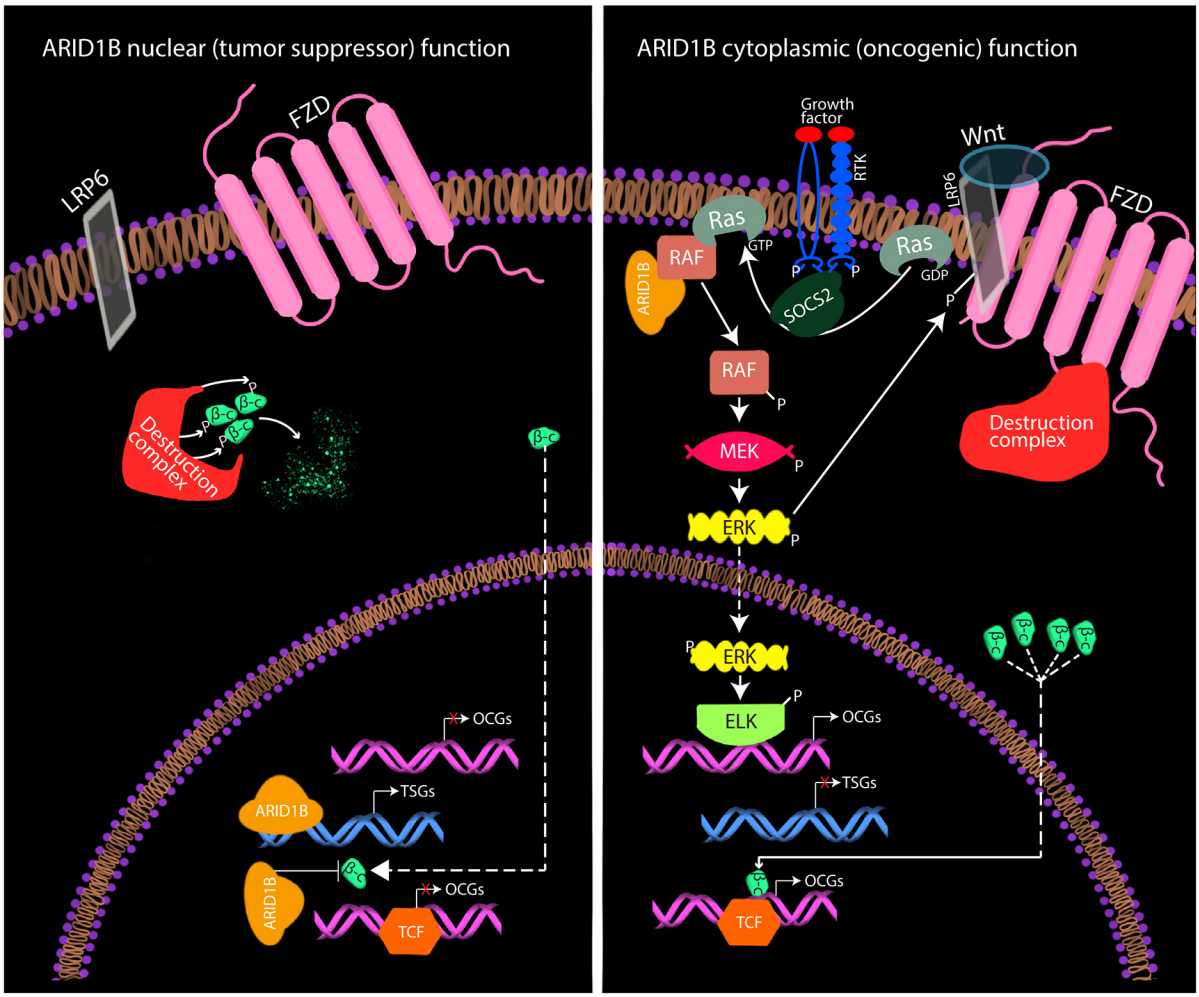

Fig. 8. The yin and yang of ARID1B; a model depicting contrasting roles for nuclear (left) and cytoplasm-localized (right) ARID1B. The canonical nuclear function of ARID1B induces transcription of classical tumor suppressor genes while repressing β-catenin-mediated transcription of oncogenes. In contrast, our current study has revealed a neo-morphic oncogenic role of cytoplasm-localized ARID1B emanating from its ability to activate ERK signaling leading to transcriptional activation of oncogenes either directly via activation of ELK or indirectly via activation of canonical Wnt–β-catenin signaling. TSGs, tumor suppressor genes; OCGs, oncogenes; β-c, β-catenin; P, phosphorylation.

monitored by microscopy and confirmed to be free of mycoplasma contamination by using a mycoplasma detection kit (Cat# B39032; Biotool, Houston, TX, USA) and DAPI staining, were authenticated using the GenePrint 10 system (Cat# 23966; Promega Corporations, Madison, WI, USA) and frozen immediately in the form of multiple independent aliquots. Each authenticated cell line was passaged fewer than five or six times before performing experiments. All cells were maintained in DMEM (Cat# SH30285.01; Hyclone, Marlborough, MA, USA) with 10% FBS (Cat# 26140-079; Thermo Fisher Scientific, Waltham, MA, USA), 1% L-glutamine (Cat# 35050-061; Thermo Fisher Scientific) and 1% antibiotic-antimycotic (Cat# 15240-062; Thermo Fisher Scientific) and transfected using polyethylenimine (PEI; Cat# 23966; Polysciences Inc., Warrington, PA, USA; used for U2OS and HEK293) or Lipofectamine 3000 (Cat# L3000015; Invitrogen, Carlsbad, CA, USA; used for MIA PaCa-2 and PANC-1), according to the manufacturer's protocol. All plasmid constructs are described in Table S6A. The ARID1B cDNA construct was a kind gift from Dr Reiko Watanabe, Tohoku University, Sendai, Japan. pDEST-N-SFB, pDEST-N-GFP, pDEST-SFB-PPP1CA and TOP/FOPFlash vectors were kind gifts from Dr M. S. Reddy, CDFD, Hyderabad, India. The mutant (G12V) KRAS cDNA construct was a kind gift from Dr S. K. Manna, CDFD, Hyderabad, India.

Subcellular fractionation was performed as previously described (Aslanian et al., 2014). The amount of nuclear and cytoplasmic fractions used in all experiments represented equal proportions of cell extract. Reverse transcription-qPCR (RT-qPCR), promoter–luciferase and MTT assays, as well as shRNA particle preparation followed by transduction, were performed as described previously (Adduri et al., 2019; Kumar et al., 2018). RT-qPCR primer sequences are available from the authors upon request. The MTT assay was also performed in the presence of MEK inhibitor (20 µM PD98,059; Cat# P215; Sigma-Aldrich) or ERK1/2 inhibitor (2 µM SCH772984; Cat# M2084; Abmole, Houston, TX, USA), or in an equal amount of DMSO.

Cell migration was examined using the Boyden chamber assay. Cells were suspended in 200 µl of DMEM medium containing 0.5% FBS and seeded on the top chamber of pre-wet Transwell inserts (24 well, 8 µm pore size; BD Biosciences, San Jose, CA, USA) at a density of 5×10^4 cells/chamber. 700 µl of complete DMEM (with 10% FBS) was added to the lower chamber as a chemoattractant, and chambers were incubated for 24 h. Cells were then washed with phosphate-buffered saline (PBS) and fixed with 4% formaldehyde for 15 min at room temperature. Cells that did not migrate through the pores were removed by a cotton swab, and inserts were stained with 0.5% Crystal Violet (2.5% w/v in methanol). The images of migrated cells were acquired using an inverted microscope (Axiovert 40 CFL, Carl Zeiss, Oberkochen, Germany) at 5× magnification from randomly selected fields. The number of migrated cells was counted from three randomly selected fields in a blind way. For

the Crystal Violet staining assay, 3×10^4 cells were seeded following transfection, cultured for 4 days, fixed using 4% paraformaldehyde and stained with 0.5% Crystal Violet.

Stable MIA PaCa-2 lines expressing the cytoplasmic form of ARID1B or empty vector were generated by transfecting pDEST-GFP-ARID1B-NLS-Mut N+C and pDEST-GFP vectors, respectively, followed by selection using neomycin (G418, 200 µg/ml; Cat# 10131027; Thermo Fisher Scientific, Waltham, MA, USA) containing medium. shRNA-based knockdown of ERK1/2 was performed exactly as previously described (Hong et al., 2009). ERK1/2 shRNA constructs were a kind gift from Dr Jong-In Park, The Medical College of Wisconsin, Milwaukee, WI, USA.

NLS prediction and computational analysis

We employed the cNLS mapper (http://nls-mapper.iab.keio.ac.jp) to predict the potential nuclear localization signal(s) of ARID1B using default settings. For comparison with the ARID1A NLS, we calculated percentage identity using EMBOSS Needle (http://www.ebi.ac.uk/Tools/psa/emboss_needle/), and the significance value of similarity was calculated as $E=Ke^{-\lambda s}$, where S is the Needleman score, and K and λ are natural scales for the search space size and the scoring system, respectively. These values are derived from PRSS (https://embnet.vital-it.ch/software/PRSS_form.html).

Senescence-associated β-galactosidase assay

Following transfection and fixation, a β-galactosidase assay was performed as described previously (Khursheed et al., 2013). Images were captured under a light microscope (EVOS XL core imaging system; Thermo Fisher Scientific) at 20× magnification. A total of 250 cells from different fields were counted for β-galactosidase positivity to estimate the number of senescent cells.

Nude mice xenograft experiments

Nude mice xenograft experiments were performed following approval from CDFD institutional animal ethics committee (protocol number EAF/MDB/CDFD/13). For the experiment, 8–9-week-old female *Foxn1*$^{-/-}$ nude mice (n=6), selected randomly, were subcutaneously injected with stable MIA PaCa2 cells (5.0×10^6) expressing either the cytoplasmic form of ARID1B or empty vector. Tumor diameters were serially measured using a digital calliper every 7 days, and tumour volumes were calculated using the formula: volume=$(W^2\times L)/2$, where W and L represent width and length, respectively. Mice were killed 6 weeks post injection by carbon dioxide euthanasia, tumors were dissected and their weight and volume were measured.

Pulldown and immunoblotting

Halo tag (Halo pulldown and labeling kit, Cat# G6500; Promega Corporations) and streptavidin bead (Cat# 17-511301; GE Healthcare Bio-Science, Uppsala, Sweden) pulldowns were performed as per standard protocol (Daniels et al., 2014; Shinde and Maddika, 2017). The eluates were resolved using SDS–PAGE, transferred onto PVDF membrane (Cat# IPVH00010; Merck Millipore, MA, USA) and probed with primary antibody at 4°C overnight. Immuno-reactive bands were detected following treatment with the appropriate secondary antibody using ECL Prime western blotting detection reagent (Cat# RPN2232; GE Healthcare Life Science).

Antibodies

Primary antibodies used for pulldown, immunoblotting, immunofluorescence (IF) and IHC were those against Halo tag (1:5000; Cat# G9211; Lot no. 0000348664; Promega Corporations), GFP (1:8000; Cat# A11122; Lot No. 2015993; Invitrogen), FLAG (1:10000; Cat# F1804; Lot No. SLBW5142; Sigma-Aldrich, MO, USA), ARID1B (IHC, 1:500; IF, 1:100; Cat# H00057492-M01; Lot No. D3291-2D2; Abnova, Taipei, Taiwan), p-ERK1/2 (1:3000; Cat# 9106S; Lot No. 30; Cell Signaling Technology; Danvers, MA, USA), ERK1/2 (1:2000; Cat# 9102; Lot No. 20; Cell Signaling Technology; Danvers, MA, USA), pAKT (1:2000; Cat# 9271L; Lot No. 13; Cell Signaling Technology), AKT (1:1000; Cat# 9272S; Lot no. 27; Cell Signaling Technology), p21 (1:5000; Cat# 2947S; Lot No. 3; Cell Signaling Technology), p27 (1:5000; Cat# 3688; Lot No. 2; Cell Signaling Technology), α-tubulin (1:8000; Cat# T6074; Lot No. 037M4804V; Sigma-Aldrich), Histone H3 (1:5000; Cat# Ab1791; Lot No. GR82485-1; Abcam, Cambridge, UK), GAPDH (1:10,000; Cat# Ab9485; Lot No. GR192141-3; Abcam), active (de-phosphorylated at Ser45) β-catenin (1:5000; Cat# 19807; Lot No. 1; Cell Signaling Technology), total β-catenin (1:10,000; Cat# 610153; Lot No. 6322806; BD Biosciences), p-c-RAF (Ser 338) (1:5000; Cat# MA5-15176; Thermo Fisher Scientific), total c-RAF (1:5000; Cat# 610151; BD Biosciences, San Jose, CA, USA), p-c-RAF (Ser 259) (1:3000; Cat# 9421; Lot No. 8; Cell Signaling Technology), BRG1/SMARCA4 (1:100; Cat# A300-813A; Lot No. 2; Bethyl, TX, USA), BAF155/SMARCC1 (1:100; Cat# A301-021A; Lot No. 1; Bethyl), BAF57/SMARCE1 (1:100; Cat# A300-810A; Lot No. 2; Bethyl) and BAF53A (1:100; Cat# A301-391A; Lot No. 1; Bethyl). Secondary antibodies used were horseradish peroxidase (HRP)-conjugated goat anti-rabbit (1:10,000; Cat# 62114038001A; Lot No. 031062; GENEI, Bangalore, India), HRP-conjugated goat anti-mouse (1:10,000; Cat# 62-6520; Lot No. SG253194; Invitrogen), Alexa Fluor 488-conjugated secondary antibody (1:200; Cat# A32723; Thermo Fisher Scientific) and Alexa Fluor 568-conjugated secondary antibody (1:200; Cat# A11036; Lot No. 1301874; Thermo Fisher Scientific). Antibodies against c-RAF and (Ser 338)p-c-RAF were generous gifts from Dr Atin Mandal, Bose Institute, Kolkatta, India. Details pertaining to validation of the antibodies are given in Table S6B.

Immunocytochemistry

Cells expressing GFP or Halo-tagged (detected using TMR direct ligand; Cat# G2991; Promega) recombinant proteins were grown on culture slides (BD Biosciences), fixed in 4% paraformaldehyde and permeabilized using 0.1% Triton X-100 (in PBS) for 10 min. Cells were washed thrice with PBS, mounted with Vectashield mounting medium (Cat# H-1200; Vector Laboratories Inc., Burlingame, CA, USA) and visualized on an LSM 700 confocal laser-scanning microscope (Carl Zeiss, Oberkochen, Germany) at 63× magnification. Images were processed and analyzed using Zen Blue software. For antibody-based staining, fixed material was incubated overnight with primary antibody at 4°C. Cells were incubated with Alexa Fluor-conjugated secondary antibody for 1 h at room temperature, mounted and visualized. For importazole treatment, cells were treated for 2 h (24 h post transfection or seeding for evaluating endogenous ARID1B) with 40 µM importazole (Cat# SML0341; Sigma-Aldrich) or an equal amount of DMSO. For the leptomycin B (LMB) assay, cells were treated for 3 h (24 h post transfection) with 20 nM LMB (Cat# L2913; Sigma-Aldrich) or an equal amount of methanol as a control.

Construction of TMA, IHC, microdissection and DNA sequencing

PaCa and breast cancer (BrCa) formalin-fixed and paraffin-embedded (FFPE) samples were procured from Krishna Institute of Medical Sciences, Hyderabad, India and Apollo Hospitals, Hyderabad, India, respectively, following approval from the institutional ethics committee. Tumor, node and metastasis (TNM) staging was determined as per the guidelines of the American Joint Committee on Cancer (AJCC). PaCa (Khursheed et al., 2013) and BrCa TMAs were constructed with at least two representative 1 mm cores from each tumor and normal sample. Several internal controls, including normal placenta, kidney, prostate, skeletal muscle and high-grade melanoma, were incorporated in the TMA for facilitating orientation and, more importantly, to avoid IHC artefacts. For IHC, 4 µm tissue sections were de-paraffinized in xylene followed by hydration through a graded series of alcohol (100%, 95%, 70%, 50%) followed by H_2O. Antigen retrieval was performed using the pressure cooker method (Norton et al., 1994) with citrate buffer (pH 6.0). Endogenous peroxidase was quenched with 3% H_2O_2 followed by primary and secondary antibody incubations for 60 and 30 min, respectively, at room temperature. Slides were counterstained with Hematoxylin, dehydrated through the graded alcohol series and mounted. Stains were visualized using the Real Envision detection system (Agilent Technologies, Santa Clara, CA, USA) as per the manufacturer's instructions. For the initial standardization of IHC, the ARID1B antibody was evaluated on sections obtained from FFPE blocks generated from MIA PaCa-2 (ARID1B null) and PANC-1 (ARID1B proficient) cells to confirm specificity of the stain. We performed analysis only on samples that were positive for ARID1B expression (Table S4). The stained sections were scored rigorously and independently by two pathologists blinded for the study. For ARID1B nuclear staining,

intensity (absent, weak, moderate and strong; 0–3 scale) and fractional epithelium staining (absent, up to 25, 50, 75 and 100%; 0–4 scale) were evaluated by the pathologist, and a sum score of 4–7 was considered positive. For ARID1B cytoplasmic staining, the pathologists provided a simple 'present' or 'absent' score given the absence of significant variation between samples. For active β-catenin and phosphorylated ERK1/2, stains were evaluated as for ARID1B and sum scores were converted as 0, negative; 1–3, low; 4–7, high.

DNA was extracted from tumor epithelium micro-dissected from FFPE sections of PaCa samples using the standard phenol-chloroform/ethanol method. The NLS encoding region was amplified using specific primers at an annealing temperature of 55°C using Amplitaq Gold (ABI Inc., CA, USA). The PCR product was sequenced using a 3100 genetic analyzer (ABI Inc., CA, USA). Primer sequences are available from the authors upon request.

Statistical analysis

All data obtained from three independent experiments were represented as mean±s.d. (unless indicated otherwise). Student's *t*-test (unpaired) was used to determine the statistical significance for all experiments, and the Fisher exact test (two-tailed) was used to calculate statistical significance of IHC data.

Acknowledgements

The ARID1B cDNA construct was a kind gift from Dr Reiko Watanabe, Tohoku University, Sendai City, Japan. Antibodies against c-RAF and (Ser 338)p-c-RAF were generous gifts from Dr Atin Mandal, Bose Institute, Kolkatta, India. pDEST-N-SFB, pDEST-N-GFP, pDEST-SFB-PPP1CA and TOP/FOPFlash vectors were kind gifts from Dr M. S. Reddy, CDFD, Hyderabad, India. The mutant (G12V) KRAS cDNA construct was a kind gift from Dr S. K. Manna, CDFD, Hyderabad, India. U2OS and HEK293 cell lines were kind gifts from Dr Rashna Bhandari, CDFD, Hyderabad, India and Dr Sangita Mukhopadhyay, CDFD, Hyderabad, India, respectively. We thank Dr Jong-In Park, The Medical College of Wisconsin, Milwaukee, Wisconsin, USA, for providing ERK1/2 shRNA constructs. We acknowledge CDFD's Sophisticated Equipment Facility for confocal microscopy and Sanger sequencing, and the Experimental Animal Facility for nude mice experiments. We thank the patients for kindly agreeing to be a part of the study. We acknowledge Dr C. Sundaram and Dr Shantveer Uppin, Nizam's Institute of Medical Sciences, Hyderabad for providing FFPE blocks of PaCa samples. We are grateful to Ms Ananya Bashyam, B.Des student, National Institute of Design, Ahmedabad, India (https://instagram.com/trespassers._will?igshid=s8d5yy8armai) for help with Fig. 8 and to Drs J. Gowrishankar, CDFD, Hyderabad, India and Geeta Narlikar, UCSF, San Francisco, CA, USA, for critical reading and important suggestions on the manuscript. Data from this manuscript was uploaded to 'bioRxiv' (https://doi.org/10.1101/830075).

Competing interests

The authors declare no competing or financial interests.

Author contributions

Conceptualization: S.A., M.D.B.; Methodology: S.A., M.D.B.; Validation: S.A., M.D.B.; Formal analysis: S.A., M.D.B.; Investigation: S.A., P.K., V.K., S.G., S.R.; Resources: S.G., M.D.B.; Data curation: S.A., M.D.B.; Writing - original draft: M.D.B.; Writing - review & editing: S.A., M.D.B.; Supervision: M.D.B.; Project administration: M.D.B.; Funding acquisition: M.D.B.

Funding

The work was supported by a grant (BT/PR13948/BRB/10/1406/2015) from the Department of Biotechnology, Ministry of Science and Technology, India, to M.D.B. S.A., a registered PhD student of Manipal Academy of Higher Education, is grateful to the Department of Science and Technology, Ministry of Science and Technology, India (DST/INSPIRE Fellowship/2012/824) for junior and senior research fellowships.

Supplementary information

Supplementary information available online at
https://jcs.biologists.org/lookup/doi/10.1242/jcs.251637.supplemental

Peer review history

The peer review history is available online at
https://jcs.biologists.org/lookup/doi/10.1242/jcs.251637.reviewer-comments.pdf

References

Adduri, R. S. R., George, S. A., Kavadipula, P. and Bashyam, M. D. (2019). SMARCD1 is a transcriptional target of specific non-hotspot mutant p53 forms. *J. Cell. Physiol.* **235**, 4559-4570. doi:10.1002/jcp.29332

Amit, S., Hatzubai, A., Birman, Y., Andersen, J. S., Ben-Shushan, E., Mann, M., Ben-Neriah, Y. and Alkalay, I. (2002). Axin-mediated CKI phosphorylation of beta-catenin at Ser 45: a molecular switch for the Wnt pathway. *Genes Dev.* **16**, 1066-1076. doi:10.1101/gad.230302

Aslanian, A., Yates, J. R., III and Hunter, T. (2014). Mass spectrometry-based quantification of the cellular response to methyl methanesulfonate treatment in human cells. *DNA Repair (Amst)* **15**, 29-38. doi:10.1016/j.dnarep.2013.12.007

Bashyam, M. D., Animireddy, S., Bala, P., Naz, A. and George, S. A. (2019). The Yin and Yang of cancer genes. *Gene* **704**, 121-133. doi:10.1016/j.gene.2019.04.025

Blagosklonny, M. V. (2002). Are p27 and p21 cytoplasmic oncoproteins? *Cell Cycle* **1**, 391-393. doi:10.4161/cc.1.6.262

Blasco, M. T., Navas, C., Martin-Serrano, G., Grana-Castro, O., Lechuga, C. G., Martin-Diaz, L., Djurec, M., Li, J., Morales-Cacho, L., Esteban-Burgos, L. et al. (2019). Complete regression of advanced pancreatic ductal adenocarcinomas upon combined inhibition of EGFR and C-RAF. *Cancer Cell* **35**, 573-587.e6. doi:10.1016/j.ccell.2019.03.002

Boulay, G., Sandoval, G. J., Riggi, N., Iyer, S., Buisson, R., Naigles, B., Awad, M. E., Rengarajan, S., Volorio, A., McBride, M. J. et al. (2017). Cancer-specific retargeting of BAF complexes by a prion-like domain. *Cell* **171**, 163-178.e19. doi:10.1016/j.cell.2017.07.036

Cervenka, I., Wolf, J., Masek, J., Krejci, P., Wilcox, W. R., Kozubik, A., Schulte, G., Gutkind, J. S. and Bryja, V. (2011). Mitogen-activated protein kinases promote WNT/beta-catenin signaling via phosphorylation of LRP6. *Mol. Cell. Biol.* **31**, 179-189. doi:10.1128/MCB.00550-10

Daniels, D. L., Méndez, J., Benink, H., Niles, A., Murphy, N., Ford, M., Jones, R., Amunugama, R., Allen, D. and Urh, M. (2014). Discovering protein interactions and characterizing protein function using HaloTag technology. Journal of visualized experiments. *J. Vis. Exp.* **89**, 51553. doi:10.3791/51553

Fujimoto, A., Totoki, Y., Abe, T., Boroevich, K. A., Hosoda, F., Nguyen, H. H., Aoki, M., Hosono, N., Kubo, M., Miya, F. et al. (2012). Whole-genome sequencing of liver cancers identifies etiological influences on mutation patterns and recurrent mutations in chromatin regulators. *Nat. Genet.* **44**, 760-764. doi:10.1038/ng.2291

Ho, L. and Crabtree, G. R. (2010). Chromatin remodelling during development. *Nature* **463**, 474-484. doi:10.1038/nature08911

Hong, S. K., Yoon, S., Moelling, C., Arthan, D. and Park, J. I. (2009). Noncatalytic function of ERK1/2 can promote Raf/MEK/ERK-mediated growth arrest signaling. *J. Biol. Chem.* **284**, 33006-33018. doi:10.1074/jbc.M109.012591

Inoue, H., Furukawa, T., Giannakopoulos, S., Zhou, S., King, D. S. and Tanese, N. (2002). Largest subunits of the human SWI/SNF chromatin-remodeling complex promote transcriptional activation by steroid hormone receptors. *J. Biol. Chem.* **277**, 41674-41685. doi:10.1074/jbc.M205961200

Inoue, H., Giannakopoulos, S., Parkhurst, C. N., Matsumura, T., Kono, E. A., Furukawa, T. and Tanese, N. (2011). Target genes of the largest human SWI/SNF complex subunit control cell growth. *Biochem. J.* **434**, 83-92. doi:10.1042/BJ20101358

Ishitani, T., Ninomiya-Tsuji, J., Nagai, S.-i., Nishita, M., Meneghini, M., Barker, N., Waterman, M., Bowerman, B., Clevers, H., Shibuya, H. et al. (1999). The TAK1-NLK-MAPK-related pathway antagonizes signalling between beta-catenin and transcription factor TCF. *Nature* **399**, 798-802. doi:10.1038/21674

Jaumot, M. and Hancock, J. F. (2001). Protein phosphatases 1 and 2A promote Raf-1 activation by regulating 14-3-3 interactions. *Oncogene* **20**, 3949-3958. doi:10.1038/sj.onc.1204526

Jiao, W., Lin, H.-M., Datta, J., Braunschweig, T., Chung, J.-Y., Hewitt, S. M. and Rane, S. G. (2008). Aberrant nucleocytoplasmic localization of the retinoblastoma tumor suppressor protein in human cancer correlates with moderate/poor tumor differentiation. *Oncogene* **27**, 3156-3164. doi:10.1038/sj.onc.1210970

Kadoch, C. and Crabtree, G. R. (2013). Reversible disruption of mSWI/SNF (BAF) complexes by the SS18-SSX oncogenic fusion in synovial sarcoma. *Cell* **153**, 71-85. doi:10.1016/j.cell.2013.02.036

Kaeser, M. D., Aslanian, A., Dong, M.-Q., Yates, J. R., III and Emerson, B. M. (2008). BRD7, a novel PBAF-specific SWI/SNF subunit, is required for target gene activation and repression in embryonic stem cells. *J. Biol. Chem.* **283**, 32254-32263. doi:10.1074/jbc.M806061200

Khursheed, M., Kolla, J. N., Kotapalli, V., Gupta, N., Gowrishankar, S., Uppin, S. G., Sastry, R. A., Koganti, S., Sundaram, C., Pollack, J. R. et al. (2013). ARID1B, a member of the human SWI/SNF chromatin remodeling complex, exhibits tumour-suppressor activities in pancreatic cancer cell lines. *Br. J. Cancer* **108**, 2056-2062. doi:10.1038/bjc.2013.200

Koster, R., di Pietro, A., Timmer-Bosscha, H., Gibcus, J. H., van den Berg, A., Suurmeijer, A. J., Bischoff, R., Gietema, J. A. and de Jong, S. (2010). Cytoplasmic p21 expression levels determine cisplatin resistance in human testicular cancer. *J. Clin. Invest.* **120**, 3594-3605. doi:10.1172/JCI41939

Kubicek, M., Pacher, M., Abraham, D., Podar, K., Eulitz, M. and Baccarini, M. (2002). Dephosphorylation of Ser-259 regulates Raf-1 membrane association. *J. Biol. Chem.* **277**, 7913-7919. doi:10.1074/jbc.M108733200

Kumar, R., Kotapalli, V., Naz, A., Gowrishankar, S., Rao, S., Pollack, J. R. and Bashyam, M. D. (2018). XPNPEP3 is a novel transcriptional target of canonical Wnt/β-catenin signaling. *Genes Chromosomes Cancer* **57**, 304-310. doi:10.1002/gcc.22531

Lange, A., McLane, L. M., Mills, R. E., Devine, S. E. and Corbett, A. H. (2010). Expanding the definition of the classical bipartite nuclear localization signal. *Traffic* **11**, 311-323. doi:10.1111/j.1600-0854.2009.01028.x

Leung, J. Y., Kolligs, F. T., Wu, R., Zhai, Y., Kuick, R., Hanash, S., Cho, K. R. and Fearon, E. R. (2002). Activation of AXIN2 expression by β-catenin-T cell factor. A feedback repressor pathway regulating Wnt signaling. *J. Biol. Chem.* **277**, 21657-21665. doi:10.1074/jbc.M200139200

Luo, J., Emanuele, M. J., Li, D., Creighton, C. J., Schlabach, M. R., Westbrook, T. F., Wong, K. K. and Elledge, S. J. (2009). A genome-wide RNAi screen identifies multiple synthetic lethal interactions with the Ras oncogene. *Cell* **137**, 835-848. doi:10.1016/j.cell.2009.05.006

Mathur, R. R. and Roberts, C. W. M. (2017). SWI/SNF (BAF) complexes: guardians of the epigenome. *Ann. Rev. Cancer Biol.* **2**, 413-427. doi:10.1146/annurev-cancerbio-030617-050151

McBride, M. J., Pulice, J. L., Beird, H. C., Ingram, D. R., D'Avino, A. R., Shern, J. F., Charville, G. W., Hornick, J. L., Nakayama, R. T., Garcia-Rivera, E. M. et al. (2018). The SS18-SSX fusion oncoprotein hijacks BAF Complex targeting and function to drive synovial sarcoma. *Cancer Cell* **33**, 1128-1141.e7. doi:10.1016/j.ccell.2018.05.002

Michel, B. C., D'Avino, A. R., Cassel, S. H., Mashtalir, N., McKenzie, Z. M., McBride, M. J., Valencia, A. M., Zhou, Q., Bocker, M., Soares, L. M. M. et al. (2018). A non-canonical SWI/SNF complex is a synthetic lethal target in cancers driven by BAF complex perturbation. *Nat. Cell Biol.* **20**, 1410-1420. doi:10.1038/s41556-018-0221-1

Morris, E. J., Jha, S., Restaino, C. R., Dayananth, P., Zhu, H., Cooper, A., Carr, D., Deng, Y., Jin, W., Black, S. et al. (2013). Discovery of a novel ERK inhibitor with activity in models of acquired resistance to BRAF and MEK inhibitors. *Cancer Discov.* **3**, 742-750. doi:10.1158/2159-8290.CD-13-0070

Norton, A. J., Jordan, S. and Yeomans, P. (1994). Brief, high-temperature heat denaturation (pressure cooking): a simple and effective method of antigen retrieval for routinely processed tissues. *J. Pathol.* **173**, 371-379. doi:10.1002/path.1711730413

Pfister, N. T., Fomin, V., Regunath, K., Zhou, J. Y., Zhou, W., Silwal-Pandit, L., Freed-Pastor, W. A., Laptenko, O., Neo, S. P., Bargonetti, J. et al. (2015). Mutant p53 cooperates with the SWI/SNF chromatin remodeling complex to regulate VEGFR2 in breast cancer cells. *Genes Dev.* **29**, 1298-1315. doi:10.1101/gad.263202.115

Plotnik, J. P., Budka, J. A., Ferris, M. W. and Hollenhorst, P. C. (2014). ETS1 is a genome-wide effector of RAS/ERK signaling in epithelial cells. *Nucleic Acids Res.* **42**, 11928-11940. doi:10.1093/nar/gku929

Reisman, D., Glaros, S. and Thompson, E. A. (2009). The SWI/SNF complex and cancer. *Oncogene* **28**, 1653-1668. doi:10.1038/onc.2009.4

Romagosa, C., Simonetti, S., López-Vicente, L., Mazo, A., Lleonart, M. E., Castellvi, J. and Ramon y Cajal, S. (2011). p16(Ink4a) overexpression in cancer: a tumor suppressor gene associated with senescence and high-grade tumors. *Oncogene* **30**, 2087-2097. doi:10.1038/onc.2010.614

Sausen, M., Leary, R. J., Jones, S., Wu, J., Reynolds, C. P., Liu, X., Blackford, A., Parmigiani, G., Diaz, L. A., Jr, Papadopoulos, N. et al. (2013). Integrated genomic analyses identify ARID1A and ARID1B alterations in the childhood cancer neuroblastoma. *Nat. Genet.* **45**, 12-17. doi:10.1038/ng.2493

Shi, J., Whyte, W. A., Zepeda-Mendoza, C. J., Milazzo, J. P., Shen, C., Roe, J.-S., Minder, J. L., Mercan, F., Wang, E., Eckersley-Maslin, M. A. et al. (2013). Role of SWI/SNF in acute leukemia maintenance and enhancer-mediated Myc regulation. *Genes Dev.* **27**, 2648-2662. doi:10.1101/gad.232710.113

Shinde, S. R. and Maddika, S. (2017) PTEN Regulates Glucose Transporter Recycling by Impairing SNX27 Retromer Assembly. *Cell Rep.* **7**, 1655-1666. doi:10.1016/j.celrep.2017.10.053

Shorstova, T., Marques, M., Su, J., Johnston, J., Kleinman, C. L., Hamel, N., Huang, S., Alaoui-Jamali, M. A., Foulkes, W. D. and Witcher, M. (2019). SWI/SNF-compromised cancers are susceptible to bromodomain inhibitors. *Cancer Res.* **79**, 2761-2774. doi:10.1158/0008-5472.CAN-18-1545

Soderholm, J. F., Bird, S. L., Kalab, P., Sampathkumar, Y., Hasegawa, K., Uehara-Bingen, M., Weis, K. and Heald, R. (2011). Importazole, a small molecule inhibitor of the transport receptor importin-β. *ACS Chem. Biol.* **6**, 700-708. doi:10.1021/cb2000296

Tordella, L., Khan, S., Hohmeyer, A., Banito, A., Klotz, S., Raguz, S., Martin, N., Dhamarlingam, G., Carroll, T., González Meljem, J. M. et al. (2016). SWI/SNF regulates a transcriptional program that induces senescence to prevent liver cancer. *Genes Dev.* **30**, 2187-2198. doi:10.1101/gad.286112.116

Vasileiou, G., Ekici, A. B., Uebe, S., Zweier, C., Hoyer, J., Engels, H., Behrens, J., Reis, A. and Hadjihannas, M. V. (2015). Chromatin-Remodeling-Factor ARID1B Represses Wnt/β-Catenin Signaling. *Am. J. Hum. Genet.* **97**, 445-456. doi:10.1016/j.ajhg.2015.08.002

Waddell, N., Pajic, M., Patch, A. M., Chang, D. K., Kassahn, K. S., Bailey, P., Johns, A. L., Miller, D., Nones, K., Quek, K. et al. (2015). Whole genomes redefine the mutational landscape of pancreatic cancer. *Nature* **518**, 495-501. doi:10.1038/nature14169

Wang, W., Xue, Y., Zhou, S., Kuo, A., Cairns, B. R. and Crabtree, G. R. (1996). Diversity and specialization of mammalian SWI/SNF complexes. *Genes Dev.* **10**, 2117-2130. doi:10.1101/gad.10.17.2117

Yan, Z., Cui, K., Murray, D. M., Ling, C., Xue, Y., Gerstein, A., Parsons, R., Zhao, K. and Wang, W. (2005). PBAF chromatin-remodeling complex requires a novel specificity subunit, BAF200, to regulate expression of selective interferon-responsive genes. *Genes Dev.* **19**, 1662-1667. doi:10.1101/gad.1323805

Ying, H., Kimmelman, A. C., Lyssiotis, C. A., Hua, S., Chu, G. C., Fletcher-Sananikone, E., Locasale, J. W., Son, J., Zhang, H., Coloff, J. L. et al. (2012). Oncogenic Kras maintains pancreatic tumors through regulation of anabolic glucose metabolism. *Cell* **149**, 656-670. doi:10.1016/j.cell.2012.01.058

Zhang, Y., Pizzute, T. and Pei, M. (2014). A review of crosstalk between MAPK and Wnt signals and its impact on cartilage regeneration. *Cell Tissue Res.* **358**, 633-649. doi:10.1007/s00441-014-2010-x